

# Toward Chemical Accuracy with Shallow Quantum Circuits: A Clifford-Based Hamiltonian Engineering Approach

Jiace Sun, Lixue Cheng, and Weitang Li\*



Cite This: *J. Chem. Theory Comput.* 2024, 20, 695–707



Read Online

ACCESS |



Metrics & More

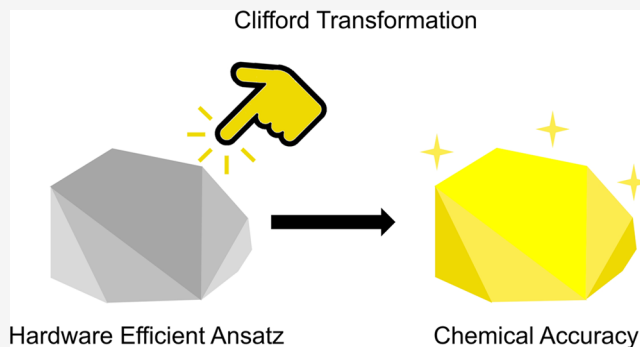


Article Recommendations



Supporting Information

**ABSTRACT:** Achieving chemical accuracy with shallow quantum circuits is a significant challenge in quantum computational chemistry, particularly for near-term quantum devices. In this work, we present a Clifford-based Hamiltonian engineering algorithm, namely CHEM, that addresses the trade-off between circuit depth and accuracy. Based on a variational quantum eigensolver and hardware-efficient ansatz, our method designs the Clifford-based Hamiltonian transformation that (1) ensures a set of initial circuit parameters corresponding to the Hartree–Fock energy can be generated, (2) effectively maximizes the initial energy gradient with respect to circuit parameters, (3) imposes negligible overhead for classical processing and does not require additional quantum resources, and (4) is compatible with any circuit topology. We demonstrate the efficacy of our approach using a quantum hardware emulator, achieving chemical accuracy for systems as large as 12 qubits with fewer than 30 two-qubit gates. Our Clifford-based Hamiltonian engineering approach offers a promising avenue for practical quantum computational chemistry on near-term quantum devices.



## 1. INTRODUCTION

In the past decade, quantum computing has been on an extraordinary trajectory of growth and development, paving the way for the quantum simulations of molecular properties.<sup>1–6</sup> A groundbreaking study in 2014 successfully simulated the HeH<sup>+</sup> molecule using a 2-qubit photonic quantum processor.<sup>7</sup> This pioneering work introduced the Variational Quantum Eigensolver (VQE) algorithm,<sup>8,9</sup> which has become the most widely adopted algorithm for the quantum simulation of molecules in the noisy intermediate-scale quantum (NISQ) era.<sup>10,11</sup> Building on this foundation, a research team from IBM in 2017 expanded the scope of quantum simulations to larger molecules, such as BeH<sub>2</sub>, by employing a 6-qubit superconducting quantum processor.<sup>12</sup> Subsequent progress in this field unlocked the potential for quantum computation to profile the chemical reaction for diazene isomerization and cyclobutene ring opening using the 54-qubit “Sycamore” quantum processor.<sup>13,14</sup> However, hindered by the limited circuit depth and hardware noise, the accuracy of these studies remained suboptimal. A recent attempt to fill this gap has reached the chemical accuracy of the LiH molecule by an optimized unitary coupled cluster (UCC) ansatz on superconducting qubits.<sup>15</sup> These achievements show the potential of quantum computing to reshape computational chemistry. As quantum hardware and algorithms evolve rapidly, it is envisioned that quantum computers will play an increasingly significant role to enhance our understanding of molecular

systems and to expedite the discovery of novel materials and drugs.<sup>16–20</sup>

The VQE algorithm is a powerful method for estimating the ground state energy of a given molecular system, leveraging the Rayleigh–Ritz variational principle.<sup>7,21,22</sup> In this approach, a parametrized quantum circuit, also referred to as an ansatz, is constructed to approximate the true ground state wave function. A quantum computer evaluates the energy expectation for a given set of circuit parameters at each iteration, and then a classical optimizer modifies the circuit parameters to minimize the energy. A critical challenge in the successful implementation of the VQE algorithm lies in the design of ansatzes that strike a balance between flexibility and simplicity.<sup>23–26</sup> Specifically, ansatzes must be capable of representing the wave function of molecular systems while remaining sufficiently simple to be efficiently implemented on quantum computers.

The UCC ansatz is initially proposed due to its clear chemical picture and close resemblance to the traditional Coupled Cluster (CC) theory.<sup>7,27</sup> The ansatz starts with a

**Received:** August 13, 2023

**Revised:** December 2, 2023

**Accepted:** December 11, 2023

**Published:** January 3, 2024



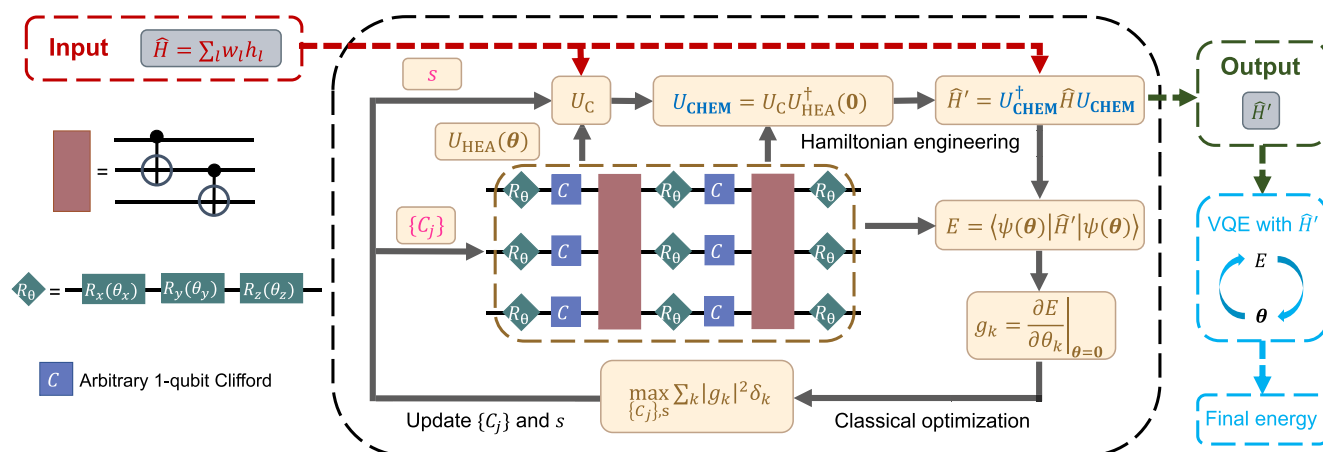


**Figure 1.** Schematic diagram for the CHEM approach. The overall objective is to find the Clifford Hamiltonian transformation  $U_{\text{CHEM}}$  to maximize the reward function  $R$  (eq 10). The parameters to optimize in the workflow are  $\{C_j\}$  and  $s$ , which are shown on the left of the flowchart and marked in magenta.  $C_j$  is single-qubit Clifford gates in the HEA circuit  $U_{\text{HEA}}(\theta)$ .  $s$  is a permutation defined by eq 19 that determines the Clifford unitary  $U_C$  based on  $U_{\text{HEA}}(\mathbf{0})$  and system Hamiltonian  $\hat{H}$ .  $U_{\text{CHEM}}$  is constructed according to eq 7, which is then used to transform the Hamiltonian  $\hat{H}$ . The energy gradient with respect to the engineered Hamiltonian  $\hat{H}'$  at  $\theta = \mathbf{0}$ , is calculated according to eq 16, which in turn determines  $R$ . The values of  $\{C_j\}$  and  $s$  are optimized by a discrete optimizer based on  $R$ . The optimal values are used to construct the engineered Hamiltonian  $\hat{H}'$  fed into the downstream VQE task.

Hartree–Fock (HF) initial state and then applies excitations to capture the correlation energy. Despite its high accuracy with only single and double excitations (UCCSD), most quantum hardware experiments are conducted using the Hardware-Efficient Ansatz (HEA)<sup>12,17,28–30</sup> or substantially simplified UCC variants<sup>7,13–15,31,32</sup> due to the deep circuit depth of UCC. The HEA family of ansatzes is specifically designed for simple implementation on NISQ devices with shallow circuits. However, the HEA approach presents its own set of challenges, often related to optimization difficulties,<sup>33,34</sup> which result in a lower accuracy compared to the UCC ansatz. For instance, random initial guesses are typically employed due to the lack of systematic methods to appropriately initialize HEA circuit parameters. Unlike the UCC ansatz, where setting all parameters to zero corresponds to initiating the VQE optimization from the HF state, selecting circuit parameters that yield the HF state as the output is nontrivial for the HEA approach. Compounding this issue, random HEA circuits are known to suffer from the “barren plateau” phenomenon, wherein gradients vanish as the number of qubits and the circuit depth increases.<sup>33</sup> Consequently, for complex molecules, it becomes challenging for HEA to even reach the HF accuracy.

There is a growing interest in designing quantum algorithms to reach the best of both worlds, i.e., to achieve chemical accuracy with shallow quantum circuits. The Adaptive Derivative-Assembled Pseudo Trotter for VQE (ADAPT-VQE)<sup>35</sup> and its variants<sup>36,37</sup> are promising approaches that balance the accuracy and circuit simplicity. These methods construct the ansatz iteratively based on the information obtained from previous VQE runs. In parallel, orbital-optimized approaches enhance the quality of a simplified UCC ansatz by optimizing molecular orbitals classically.<sup>38–40</sup> While both ADAPT-VQE and orbital-optimized approaches demonstrate improvements in accuracy and circuit depth, they may inadvertently increase the measurement cost associated with VQE.

In this study, we present a Hamiltonian engineering approach to address the trade-off between circuit depth and

accuracy in quantum computational chemistry. Our method exploits the property that any unitary transformation applied to the Hamiltonian preserves its eigenspectrum. Based on HEA circuits, the Hamiltonian transformation is designed to 1) ensure that a set of initial circuit parameters that correspond to the HF energy can be generated; 2) maximize the energy gradient with respect to circuit parameters; 3) impose negligible overhead for classical processing without input from quantum computers; and 4) be compatible with any HEA circuit topology. As these objectives are achieved by virtue of the Gottesman–Knill theorem for Clifford circuits,<sup>41,42</sup> we term this Clifford-based Hamiltonian Engineering approach for Molecules as CHEM. Experimental results obtained from a quantum hardware emulator provide compelling evidence of our method’s efficacy. Remarkably, it achieves chemical accuracy for systems as large as 12 qubits, using quantum circuits with fewer than 30 two-qubit gates and linear qubit connectivity. To the best of our knowledge, such a level of performance has not been previously reported in the literature.

## 2. THEORY AND METHOD

In this section, we first provide an overview of the basic concepts of VQE, HEA, and the Clifford group in Sec. 2.1 and present our proposed Hamiltonian engineering approach for accurately estimating molecular energy with shallow circuits in Sec. 2.2–Sec. 2.5.

**2.1. VQE, HEA, and the Clifford Circuit.** In this work, we consider the molecular electronic structure Hamiltonian in the second-quantized form

$$\hat{H} = \sum_{pq} v_{pq} \hat{a}_p^\dagger \hat{a}_q + \frac{1}{2} \sum_{pqrs} v_{pqrs} \hat{a}_p^\dagger \hat{a}_q^\dagger \hat{a}_r \hat{a}_s \quad (1)$$

where  $v_{pq}$  and  $v_{pqrs}$  are one-electron integrals and two-electron integrals, respectively.  $\hat{a}^\dagger$  and  $\hat{a}$  are Fermionic creation and annihilation operators. In order to measure the expectation of  $\hat{H}$  on a quantum computer, the Hamiltonian is converted into a summation of  $N$ -qubit Pauli string

$$\hat{H} = \sum_l^{N_H} w_l h_l \quad (2)$$

where  $w_j$  is real coefficients,  $N_H$  is the total number of terms, and  $h_l = \sigma_{i_1} \otimes \sigma_{i_2} \otimes \dots \otimes \sigma_{i_N}$  with  $\sigma_{i_k} \in \{X, Y, Z, I\}$ .

The wave function of the molecular system, represented by a parametrized quantum circuit  $U(\theta)$ , can be written as

$$|\psi(\theta)\rangle = U(\theta)|\phi\rangle \quad (3)$$

where the initial state  $|\phi\rangle$  is usually a product state. The molecular energy with given parameters  $E(\theta) = \langle\psi(\theta)|\hat{H}|\psi(\theta)\rangle$  can then be computed using a quantum computer. The goal of VQE is to find a set of optimal parameters  $\theta^*$  that minimizes  $E$  using classical optimizers.

HEA is a family of versatile and widely used ansatzes that is particularly suitable for execution on near-term quantum hardware.<sup>43</sup> Compared with the UCC type of ansatz, the HEA type ansatz has a lower circuit depth by utilizing hardware connectivity and maximizing the number of operations at each layer. Typically, HEA is composed of interleaved single-qubit rotation gate layers  $L_{\text{rot}}^{(l)}(\{\theta_{lj}\})$  and entangler gate layers  $L_{\text{ent}}^{(l)}$ . An HEA circuit with  $p$  layers can be expressed as

$$U_{\text{HEA}}(\{\theta_{lj}\}) := \prod_{l=p}^1 [L_{\text{rot}}^{(l)}(\{\theta_{lj}\})L_{\text{ent}}^{(l)}]L_{\text{rot}}^{(0)}(\{\theta_{0j}\}) \quad (4)$$

Note that the product  $\prod_{l=p}^1$  is written in a reverse order to match the direction of the circuit, i.e., the gates with smaller indices are applied first. Single qubit rotation layer  $L_{\text{rot}}(\{\theta_{nj}\})$  can generally be written as  $L_{\text{rot}}^{(l)}(\{\theta_{lj}\}) = \prod_{j=M}^1 R_j(\theta_{lj})$  with  $R_j(\theta) = \exp(i\frac{\theta}{2}P_j)$  and  $P_j \in \{X, Y, Z\}$ . It follows that  $L_{\text{rot}}^{(l)}(\{\theta_{lj} = 0\}) = I$ . The form of  $L_{\text{ent}}^{(l)}$  is rather flexible, and an example with consecutive CNOT gates and arbitrary Clifford gates  $\{C_j\}$  is illustrated in the brown dashed box in Figure 1. A key feature of  $L_{\text{ent}}^{(l)}$  is that they are typically Clifford circuits, which enables the Clifford-based Hamiltonian engineering approach for molecules (CHEM) described below.

Clifford circuits are a special class of quantum circuits that consist of gates from the Clifford group, which is a subgroup of the unitary group. The Clifford group is generated by three gates: the Hadamard gate ( $H$ ), the phase gate ( $S$ ), and the controlled-NOT gate (CNOT). If  $C$  is a Clifford operator, then for any Pauli string  $P$ ,  $C^\dagger P C$  is still a Pauli string. The ability to classically simulate Clifford circuits stems from the Gottesman-Knill theorem, which states that any quantum circuit composed solely of Clifford gates and measurements in the computational basis can be efficiently simulated on a classical computer using the stabilizer formalism.<sup>41,42</sup> The classical simulation complexity of Clifford circuits without measurements is  $O(N)$  in the number of qubits  $N$ , as opposed to the exponential complexity associated with simulating general quantum circuits.

**2.2. Clifford-Based Hamiltonian Engineering.** In this section, we introduce how to design the Hamiltonian transformation  $U_{\text{CHEM}}$  to facilitate the optimization of HEA circuits. The overall workflow is depicted in Figure 1.

The transformed Hamiltonian  $\hat{H}'$  is defined as

$$\hat{H}' = U_{\text{CHEM}}^\dagger \hat{H} U_{\text{CHEM}} \quad (5)$$

$\hat{H}'$  shares the same eigenspectrum with  $\hat{H}$  but with different eigenstates. We restrict  $U_{\text{CHEM}}$  to be Clifford operation, so that

$\hat{H}'$  can be efficiently processed on a classical computer and  $\hat{H}'$  has the same number of terms with  $\hat{H}$ . We first let  $U_{\text{CHEM}} = U_{\text{HEA}}^\dagger(\mathbf{0})$  and set the initial state of the circuit  $|\phi\rangle$  as the Hartree–Fock state  $|\psi_{\text{HF}}\rangle$ . Then, the energy expectation at  $\theta = \mathbf{0}$  is

$$\langle\psi(\mathbf{0})|\hat{H}'|\psi(\mathbf{0})\rangle = \langle\psi_{\text{HF}}|\hat{H}|\psi_{\text{HF}}\rangle \quad (6)$$

Within this transformation, the HEA circuit reaches HF energy by setting  $\theta = \mathbf{0}$ , which serves as a good starting point for subsequent parameter optimization.

Then, we take one step further by introducing an extra freedom  $U_C$  to  $U_{\text{CHEM}}$

$$U_{\text{CHEM}} = U_C U_{\text{HEA}}^\dagger(\mathbf{0}) \quad (7)$$

where  $U_C$  is an arbitrary Clifford operator with the only restriction that it is invariant to the HF state, i.e.,  $U_C|\psi_{\text{HF}}\rangle = e^{i\alpha}|\psi_{\text{HF}}\rangle$  up to some global phase factor  $e^{i\alpha}$ . This is necessary for eq 6 to still hold. Here,  $U_C$  is allowed to be dependent on the structure of  $U_{\text{HEA}}$ .

In order to find better estimations of the ground state energy, we construct  $U_C$  by maximizing the energy gradients at  $\theta = \mathbf{0}$ . Maximizing energy gradients has been proven to be a reliable approach toward compact circuit ansatz and efficient Hamiltonian transformation.<sup>35,44</sup>

To simplify notation, we rewrite the HEA in eq 4 as

$$U_{\text{HEA}}(\theta) = \prod_{j=M}^1 R_j(\theta_j) B_j \quad (8)$$

where  $B_j$  is a (multiqubit) Clifford operator (could also be identity). We note that eq 8 is not restricted to the HEA structure in Figure 1; thus, our method can also be applied to other types of HEA as well. According to the simplified indices in eq 8, the energy derivative is written as

$$g_k = \partial_{\theta_k} E(\mathbf{0}) = \left. \frac{\partial E}{\partial \theta_k} \right|_{\theta=\mathbf{0}} \quad (9)$$

The reward function that we seek to maximize is defined as

$$R = \sum_k |g_k|^2 \delta_k \quad (10)$$

where  $\delta_k = 0$  or 1 indicates whether the gradient is redundant due to linear dependencies in  $\{\partial_{\theta_k}|\psi(\mathbf{0})\rangle\}$ . For example, if two of the tangent vectors are linearly dependent, the corresponding parameters are redundant during the optimization. Thus, only one of them should be kept in the reward function. In principle, higher-order derivatives, such as  $h_{kl} = \partial_{\theta_k} \partial_{\theta_l} E(\mathbf{0})$ , can also be included in  $R$ , which shall be the subject of our future work.

Next, we present simplified expressions for  $g_k$  and  $\delta_k$ . To begin with, we define Pauli string  $Q_k$  that is transformed from the Pauli operator  $P_k$  associated with the  $k$ th rotation gate  $R_k$ :

$$Q_k = \prod_{j=1}^k B_j^\dagger P_k \prod_{j=k}^1 B_j \quad (11)$$

$Q_k$  can be efficiently calculated on a classical computer since  $B_j$  is Clifford. The wave function derivatives are then written as

$$\partial_{\theta_k} |\psi(\mathbf{0})\rangle = -\frac{i}{2} U_{\text{HEA}}(\mathbf{0}) Q_k |\psi_{\text{HF}}\rangle \quad (12)$$

Using eq 12,  $\delta_k$  in eq 10 is determined as follows. The overlaps between  $\{\partial_{\theta_k}|\psi(\mathbf{0})\}$  are

$$s_{kl} = \langle \partial_{\theta_k} \psi(\mathbf{0}) | \partial_{\theta_l} \psi(\mathbf{0}) \rangle = \frac{1}{4} \langle \psi_{\text{HF}} | Q_k Q_l | \psi_{\text{HF}} \rangle \in \left\{ \pm \frac{1}{4}, \pm \frac{i}{4}, 0 \right\} \quad (13)$$

Thus, we let  $\delta_k = 0$  if  $s_{kl} = \pm \frac{1}{4}$  for some  $l < k$ , and  $\delta_k = 1$  otherwise.

On the other hand, the energy derivatives are

$$g_k = \sum_{l=1}^{N_H} w_l \text{Im}[\langle \psi_{\text{HF}} | h'_l Q_k | \psi_{\text{HF}} \rangle] \quad (14)$$

with  $h'_l = U_C^\dagger h_l U_C$ . Formally, eq 14 reduces to the expression of energy gradients iterative qubit coupled cluster (iQCC) approach<sup>45,46</sup> when the circuit is simply  $e^{-i\theta Q_k/2}$ . However, unlike iQCC, in which case the goal is to find a series of  $\{Q_k\}$  and construct the circuit based on  $\{Q_k\}$ , our method targets  $U_C$  to avoid breaking the HEA circuit topology.

Based on eq 12 and eq 14, it is straightforward to calculate  $R$  once  $U_C$  is known. However, the reversed task of finding  $U_C$  that maximizes  $R$ , given  $\hat{H}$  and  $\{Q_k\}$ , is considerably more complex. In this work, we propose a heuristic greedy algorithm designed to address this challenge. The details of the algorithm extend beyond the fundamental concept of CHEM outlined above and will be presented in the subsequent section.

To summarize this section, we briefly recap the key idea of CHEM by analyzing how CHEM changes the landscape of HEA. Both traditional HEA and HEA with CHEM can be viewed as a parametrized ansatz that maps to a subspace of the entire wave function space. However, traditional HEA effectively chooses a random subspace, while CHEM tries to find the optimal subspace by maximizing the energy derivatives at the HF state. Since the subspace dimension is exponentially small compared with the full space, randomly choosing the subspace can be expected to give only exponentially small energy improvements. In contrast, a subspace with large energy derivatives ensures that at least a decent local minimum can be reached. To ensure a global minimum, we need to consider the infinite order of derivatives at  $\theta = \mathbf{0}$ . The current approach of using only gradients can be viewed as a first-order approximation.

**2.3. An Efficient Algorithm for Finding  $U_C$ .** In this section, we describe a greedy algorithm for finding  $U_C$ , which proves effective in our numerical experiments. We will start by simplifying the expression of  $R$  using the binary representation of Pauli strings. Next, we propose a greedy algorithm that constructs  $U_C$  based on the HEA circuit structure and the Hamiltonian. The whole algorithm is outlined in Algorithm 1. We also present a simple 2-qubit example to demonstrate the algorithm in Figure 2. We note that the whole process is carried out efficiently on classical computers without any input from quantum computers, and a complexity analysis is provided at the end of the section.

Without loss of generality, we assume  $|\psi_{\text{HF}}\rangle = |0\rangle^{\otimes n}$ , and then, the expectation in eq 14 can be simplified by

$$\langle \psi_{\text{HF}} | P Q | \psi_{\text{HF}} \rangle = \begin{cases} (-1)^{z_Q \cdot x_Q} \phi_P \phi_Q & \text{if } x_P = x_Q \\ 0 & \text{else} \end{cases} \quad (15)$$

for arbitrary Pauli operators  $P$  and  $Q$ , where  $x$ ,  $z$ , and  $\phi$  are binary representations of Pauli operators. Specifically, for Pauli operator  $P$  we have  $P = \phi_P \prod_i (Z[i])^{z[i]} (X[i])^{x[i]}$ , where  $\phi_P \in$

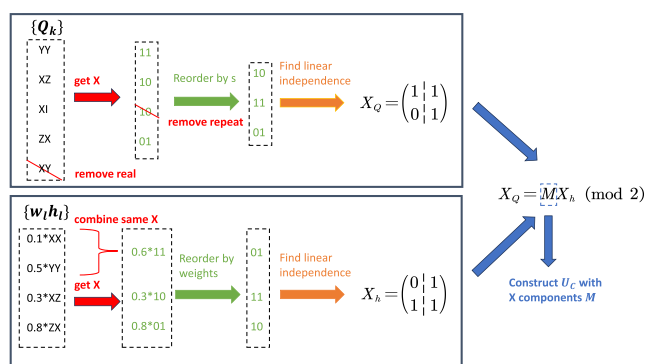


**Figure 2.** A simple 2-qubit example demonstrating the greedy algorithm to find Clifford transformation  $U_C$ .  $\{h_l\}$  and  $\{w_l\}$  are the Pauli terms and weights of the Hamiltonian, respectively, while  $\{Q_k\}$  is constructed by eq 11. The first step (marked in red) is to make some simplifications for  $\{h_l\}$  and  $\{Q_k\}$  by (1) removing  $Q_k$  with real phases or repeated  $X$  components and (2) combining  $\{h_l\}$  with the same  $X$  components. We note that the  $X$  component of  $0.1XX + 0.5YY$  is  $0.4$  since  $YY = (-iZX)$  has an opposite sign with  $XX$ . The second step (marked in green) is to reorder the  $X$  components of  $\{Q_k\}$  and  $\{h_l\}$  by permutation  $s$  and weights  $w_l$ , respectively. The third step (marked in orange) is to use Gaussian elimination to find linear independent terms to construct  $X_h$  and  $X_Q$ . Finally, we solve  $M$  and construct  $U_C$  with  $X$  components  $M$ .

$\{1, i, -1, -i\}$ ,  $x[i]_p \in \{0, 1\}$ ,  $z[i]_p \in \{0, 1\}$ . The index in the square parentheses is the qubit index.  $x_p$  and  $z_p$  are the vector representations of  $\{x[i]_p\}$  and  $\{z[i]_p\}$ . Using this representation,  $PQ$  can be expressed as  $\phi_P \phi_Q \prod_i (Z[i])^{z[i]_p} (X[i])^{x[i]_p} (Z[i])^{z[i]_q} (X[i])^{x[i]_q}$ . With the anti-commutation relationships of  $X$  and  $Z$ , eq 15 then follows naturally.

Eq 15 allows us to simplify the calculation of the reward function  $R$  in eq 10 from the following aspects one by one. The first aspect involves screening out terms with zero contributions in the summation in eq 10. Since  $\phi_{h_l}$  is always real,  $\langle \psi_{\text{HF}} | h'_l Q_k | \psi_{\text{HF}} \rangle$  in eq 14 has an imaginary part only when  $Q_k$  has an imaginary part. Thus, indices  $k$  with  $\phi_{Q_k} \neq \pm i$  can be dropped in eq 10 since the corresponding  $g_k$  is zero. Second, from eq 13,  $s_{kl} = \pm \frac{1}{4}$  is equivalent to  $x_{Q_k} = x_{Q_l}$ . Thus, the  $\delta_k$  factor in eq 10 essentially removes repeating  $x_{Q_l}$  vectors, and in the following, we may assume  $x_Q$  is unique. The third aspect is more for notational simplicity. Specifically, we combine those  $h'_l$  with the same  $x_{h'_l}$  and keep only one of them. Meanwhile, the weights  $w_l$  are summed accordingly with the phase information from  $\phi_{h_l}$  taken into account. This is viable because  $z_p$  does not appear in eq 15, and  $h'_l$  with the same  $x_{h'_l}$  has the same  $\langle \psi_{\text{HF}} | h'_l Q_k | \psi_{\text{HF}} \rangle$ . Consequently, we may also assume  $x_{h'}$  is unique. The treatment is similar to the Hamiltonian partitioning process in the iQCC algorithm<sup>45,46</sup> but simpler due to the stronger  $|\psi_{\text{HF}}\rangle = |0\rangle^{\otimes n}$  assumption we have. After these operations,  $g_k$  and  $R$  become

$$g_k = \begin{cases} \pm w_l & \text{if } x_{Q_k} = x_{h'_l} \text{ for some } l \\ 0 & \text{otherwise} \end{cases} \quad (16)$$

$$R = \sum_{l \in \{l | x_{h'_l} \in \{x_{Q_k}\}\}} |w_l|^2 \quad (17)$$

where  $|w_l|$ ,  $x_{h_i}$ , and  $x_{Q_k}$  are after the above simplifications (the same hereinafter). Note that there is at most one  $x_{h_i}$  that satisfies  $x_{Q_k} = x_{h_i} \cdot g_k$  and  $R$  only depend on  $|w_l|$ ,  $x_{h_i}$ , and  $x_{Q_k}$ . The theoretical upper limit of  $R$  is  $R_{\max} = \sum_l |w_l|^2$ , which is achieved when  $\{x_{h_i}\} \subseteq \{x_{Q_k}\}$ .

Next, we present an efficient algorithm to find  $U_C$  that approximately maximizes  $R$ . Under the stabilizer formalism, a Clifford operator is uniquely specified up to a global phase by its transformation result of  $\{Z[1], Z[2], \dots, Z[N]\}$  and  $\{X[1], X[2], \dots, X[N]\}$ . Therefore, requiring  $U_C|\psi_{\text{HF}}\rangle = e^{i\alpha}|\psi_{\text{HF}}\rangle$  means that  $U_C^\dagger Z[i] U_C$  only has  $Z$  components in the binary representation. As a consequence,  $U_C^\dagger X[i] U_C$  must have only  $X$  components since Clifford transformation preserves commutation/anticommutation relations. Since we do not care about the signs,  $U_C$  can be specified by  $M \in \mathbb{Z}_2^{N \times N}$  such that  $U_C^\dagger X[i] U_C$  has  $X$  component  $M_i$  (the  $i$ th row of  $M$ ) in the binary representation. This allows us to relate  $x_{h_i}$  and  $x_{h_i}$  by

$$x_{h_i} = Mx_{h_i} \quad (18)$$

Supposing the matrix forms of  $x_h$  and  $x_Q$  are  $X_h \in \mathbb{Z}_2^{N_h \times N_h}$  and  $X_Q \in \mathbb{Z}_2^{N_Q \times N_Q}$ , where  $N_h$  and  $N_Q$  are the number of  $h$  and  $Q$ , respectively, maximizing eq 17 is equivalent to finding  $M$  such that  $X'_h = MX_h$  has the most repeated columns with  $X_Q$  weighted by  $|w_l|^2$ . On the other hand, the transformation for  $\{Z[1], Z[2], \dots, Z[N]\}$ , which does not affect  $R$ , is determined by  $M$  up to a phase because Clifford transformation preserves commutation/anticommutation relations.

Although the problem of finding  $M$  described above is more tractable than “finding the best  $U_C$ ”, it still represents a discrete optimization problem, which is generally difficult to solve. In the following, we describe a greedy algorithm for this maximization problem, which proves effective in our numerical simulation. The algorithm is motivated by the fact that any two full-rank  $n \times r$  matrices can be related by an  $n \times n$  invertible transformation  $M$ . Specifically, let the rank of  $X_h$  be  $r_h$ , the rank of  $X_Q$  be  $r_Q$ , and  $r = \min(r_h, r_Q)$ . Then, we greedily find  $r$  linearly independent columns of  $X_h$  as  $X_h^r \in \mathbb{Z}_2^{N_h \times r}$  with the largest weights  $|w_l|^2$  and find  $r$  linearly independent columns of  $X_Q$  as  $X_Q^r \in \mathbb{Z}_2^{N_Q \times r}$ . The searching of linearly independent columns can be done using Gaussian elimination with modulo 2. Since  $X_h^r$  and  $X_Q^r$  are full-rank, we can easily construct  $M \in \mathbb{Z}_2^{N_h \times N_h}$  such that  $MX_h^r = X_Q^r$ . Thus, it is guaranteed to achieve  $R \geq \sum_{i=1}^r |w_{h_i}^r|^2$ , where  $w_{h_i}^r$  is the corresponding weights of  $X_h^r$ . In Algorithm 1, we present the pseudocode for constructing  $M$  based on the greedy algorithm.

Since the  $r$  linearly independent columns of  $X_Q$  are not unique, we may optimize the columns chosen such that  $R$  is maximized. To do this, we reorder the columns of  $X_Q$  by a permutation  $s$

$$s : x_{Q_i} \rightarrow x_{Q_{s(i)}} \quad (19)$$

before the Gaussian elimination and allow  $s$  to change freely. Furthermore, we permit the single-qubit Clifford gates  $\{C_j\}$  shown in Figure 1 to vary freely among all 24 different single-qubit Clifford operators. Although these gates do not generate entanglement in the quantum state, they allow  $Q_k$  to traverse the Pauli string space and, eventually, help to shape the optimization landscape such that a high-quality local minimum can be reached easily. The parameters  $s$  and  $\{C_j\}$  can be

Algorithm 1: A greedy algorithm for finding  $U_C$

```

input : Hamiltonian  $\hat{H}$  (Eq. 2) and quantum circuit  $U_{\text{HEA}}(0)$  (Eq. 8)
output: Clifford unitary transformation  $U_C$ 

1 Construct  $X_h$  from  $\hat{H}$ 
2 Combine repeated  $x_{h_i}$  in  $X_h$  with summed weights  $w_l$ 
3 Reorder columns of  $X_h$  based on weights  $|w_l|$ 
4  $X_h = \text{GaussianElimination}(X_h)$ 
5  $X_h^r = X_h[:, :r]$  /* The first  $r$  columns */
6 while not converged do
7   Generate new  $s$  and  $\{C_j\}$ 
8   /*  $Q_k$  is determined by the quantum circuit */
9   Construct  $\{Q_k\}$  from  $U_{\text{HEA}}(0)$  and  $\{C_j\}$  based on Eq. 11
10  Drop  $Q_k$  with real  $\phi_{Q_k}$  or repeated  $x_{Q_k}$ 
11  Construct  $X_Q$  from  $\{Q_k\}$ 
12   $r = \text{Min}(\text{Rank}(X_h), \text{Rank}(X_Q))$ 
13  Reorder columns of  $X_Q$  based on  $s$ 
14   $X_Q = \text{GaussianElimination}(X_Q)$ 
15   $X_Q^r = X_Q[:, :r]$  /* The first  $r$  columns */
16   $M = X_Q^r \cdot \text{PseudoInverse}(X_h^r)$ 
17  Calculate  $R$  based on Eq. 17
18 end
19 Construct  $U_C$  based on  $M$ 

```

optimized by some classical discrete optimizer. The overall workflow for Clifford-based Hamiltonian engineering, illustrated in Figure 1, is as follows. At the beginning of each optimization step, we input a list of single-qubit Clifford gates  $\{C_j\}$  and permutation  $s$ . Subsequently, we obtain  $\{Q_k\}$  using eq 11.  $\{Q_k\}$  and  $s$ , combined with the Hamiltonian  $H = \sum_l w_l |h_l\rangle$ , are then used to generate the Clifford transformation  $U_C$  by the aforementioned greedy algorithm. After that, the Hamiltonian is transformed according to eq 5. Finally, we calculate the reward function  $R$  using eq 17 and update  $\{C_j\}$  and  $s$  for the next iteration. After the optimization is complete, VQE with the engineered  $\hat{H}'$  is performed to calculate the molecular energy. It is worth noting that the discrete optimization over  $s$  and  $C_j$  is not the key component of CHEM. Rather, the greedy algorithm, which constructs  $U_C$  from given  $s$  and  $\{C_j\}$ , is the primary driver behind the success of CHEM. In Table 2, we show that based on random  $s$  CHEM significantly improves the  $R_y$  ansatz.

Lastly, we discuss the computational cost complexity of this algorithm in each iteration. We recall that  $p$  is the number of layers so there are  $O(Np)$  single-qubit rotations and CNOT gates. To calculate  $Q_k$ , we need to do  $O(Np)$  Clifford evolutions, which have cost  $O(N^2p)$ . The cost of performing the Gaussian eliminations for  $X_Q$  is  $O(N^3p)$ . We note that Gaussian elimination for  $X_h$  is only needed to be performed once so is not counted in the cost of each iteration here. Thus, the total cost is finally  $O(N^3p)$ . We note that a direct calculation of eq 14 is  $O(N^4)$  for each  $g_k$ , which would lead to an overall scaling of  $O(N^3p)$ . By simplifying eq 14 to eq 16, the computational complexity for each  $g_k$  is reduced to  $O(\log N^4) < O(N)$  through a binary search. Therefore, its contribution to the final scaling can be neglected. Given that the entire iteration is executed on classical computers with low scaling with  $N$ , the CHEM method accelerates the subsequent VQE with minimal additional preprocessing overhead.

**2.4. Relation with Previous Works.** CHEM engineers the Hamiltonian via Clifford similarity transformation and outputs a Clifford-initialized circuit for VQE. Here, we compare and discuss the relation of CHEM with previous works that either use Hamiltonian similarity transformation or Clifford initialization techniques for VQE problems, respectively.

Both the iQCC approach<sup>45,47–49</sup> and CHEM aim at reducing the circuit depth by maximizing the first-order energy derivatives in eq 14. However, the iQCC approach selects the best  $\{Q_k\}$  and constructs the circuit with the form  $e^{-i\theta Q_k/2}$ ,

which generally decomposes to  $\sim 2N$  (where  $N$  is the number of qubits) linearly connected CNOT gates and does not fully utilize the HEA topology. Compared with iQCC, CHEM focuses on finding the best Clifford transformation  $U_{\text{CHEM}}$  instead of  $\{Q_k\}$ , which does not require any decomposition of multiqubit gates while allowing user-specified or hardware-specific HEA circuit topology. Additionally, the iQCC approach involves an iterative transformation of the Hamiltonian using multiqubit rotation gates, resulting in a growth of terms in the Hamiltonian and thus a higher measurement cost. CHEM does not have this issue since the transformation is fully Clifford. Furthermore, since Clifford transformations preserve commutation properties, the number of mutually commuting groups for the Hamiltonian remains the same after the transformation. As a result, assuming entangled measurements, the number of measurement shots does not increase. On the other hand, it is possible that the Pauli string becomes more nonlocal if the Bravyi-Kitaev transformation is employed, which will result in a deeper measurement circuit.

A recent study employed hierarchical Clifford similarity transformations to reduce entanglement in the wave function.<sup>50</sup> The method is tested for VQE tasks and shows promising results. In contrast, CHEM engineers Clifford similarity transformation by directly targeting optimized VQE energies. Clifford transformation has also been utilized to entangle independent quantum circuits for VQE.<sup>51</sup> In all aforementioned methods, the transformation over  $\hat{H}$  is built iteratively using information from expensive trial VQE runs. In contrast, CHEM constructs the overall transformation  $U_{\text{CHEM}}$  on a classical computer using the efficient algorithm proposed in Sec. 2.2.

CHEM optimizes  $\{C_j\}$  in the HEA circuit, which shows resemblance to the Clifford circuit initialization methods.<sup>52,53</sup> These approaches aim to improve VQE performance by optimizing circuit architecture classically, requiring the initial circuit to be composed of Clifford gates. The optimization objective is either the energy or its derivatives. However, without a proper engineering of  $U_C$ , the number of required trials exponentially increases with increasing the number of qubits to find a set of optimal  $\{C_j\}$  with nonzero  $g_k$  by a brute force search. To see this, we can assume that the Pauli operator  $Q$  calculated from eq 11 is randomly distributed in all  $N$ -qubit Pauli operators, and then, the probability that  $g = \text{Im}[\langle \psi_{\text{HF}} | hQ | \psi_{\text{HF}} \rangle]$  gives a nonzero value for some fixed  $h$  decays as  $2^{-N}$ . Thus, it is crucial to match  $x_h$  and  $x_Q$  via the Clifford Hamiltonian engineering proposed in Sec. 2.2. Failing to do so would merely transfer the difficulty in VQE optimization to the challenge of optimizing Clifford gates.

**2.5. Numerical Details.** In this study, all the HEA simulations are performed using the TENCIRCHEM package<sup>54</sup> with inputs computed using the CHEM package (<https://github.com/sherrylixuecheng/CHEM>). The molecular integrals and reference energies based on classical computational chemistry are obtained via the PySCF package.<sup>55</sup> The parity transformation<sup>56,57</sup> with two-qubit reduction is employed to convert the Hamiltonian defined by eq 1 into a summation of Pauli strings. The calculations of  $g_k$  and  $R$  are implemented by JAX<sup>58</sup> with just-in-time compilations. The discrete values of  $C_j$  and  $s$  are optimized by the simulated annealing (SA) method. Practically, we use  $\sqrt{R}$  instead of  $R$  as the objective function. In each step of SA, we make a trial move by randomly changing one value of  $C_j$  and randomly switching two elements in  $s$ . For a given circuit with  $N$  qubits and  $p$  layers, we perform the SA

optimizations by  $50 * N * p$  iterations, and the corresponding temperatures in the SA optimizations decrease from 0.05 to 0.002 evenly on a logarithmic scale. Due to the efficient algorithm proposed in Sec. 2.2, the whole iteration terminates within seconds for the systems tested in this work. To obtain the final HEA energies, we use the L-BFGS-B optimizer implemented in the SciPy package<sup>59</sup> with the default settings to optimize the HEA circuits engineered by CHEM.

### 3. RESULTS AND DISCUSSION

We show the ability of CHEM to reach high accuracy with shallow circuits by simulating four molecules and seven

**Table 1. Molecular Systems Tested in This Work<sup>a</sup>**

Molecule	Geometry	Active space
H <sub>4</sub>	$d = 0.8000 \text{ \AA}$	(2e, 3o), $1a_{1u}$ , $2a_{1g}$ , $2a_{1u}$ full space
LiH	$d = 1.600 \text{ \AA}$	(2e, 3o), $2a_1$ , $3a_1$ , $4a_1$ full space
BeH <sub>2</sub>	$d = 1.000 \text{ \AA}$	(4e, 4o), $2a_{1g}$ , $1a_{1u}$ , $3a_{1g}$ , $2a_{1u}$ full space
H <sub>2</sub> O	$d = 0.9584 \text{ \AA}$ , $\phi = 104.45^\circ$	(4e, 4o), $3a_1$ , $1b_2$ , $4a_1$ , $2b_1$

<sup>a</sup> $d$  is the bond length, and  $\phi$  is the bond angle. The STO-3G basis set is used throughout.

electronic structure systems numerically. The molecular systems tested in this study are summarized in Table 1. In this work, the results collected on BeH<sub>2</sub> systems are demonstrated and discussed extensively. With the STO-3G basis set and parity transformation, BeH<sub>2</sub> corresponds to 7 spatial orbitals and 12 qubits. We also employ a (4e, 4o) active space description of the BeH<sub>2</sub> with all valence electrons and  $A_1$  orbitals.

**3.1. Validity of Reward Function  $R$  and Necessity of  $U_C$ .** Figure 3 demonstrates how engineering the Hamiltonian can result in lower VQE-optimized energy by maximizing the reward  $R$ . The data points are obtained from 1000 random runs of simulated annealing. Across all subfigures in Figure 3, the optimized energy errors are well correlated with the reward  $R$  for a Hamiltonian transformation  $U_{\text{CHEM}}$ , indicating that the design of  $R$  is a valid proxy to the quality of the corresponding VQE problem. That is, the better  $R$  we achieve, the lower energy we can reach in the subsequent VQE. Furthermore, compared with the approach in which  $U_C$  is assumed to be identity and only  $\{C_j\}$  is optimized, which is shown in Figure 3(c) and (d), our engineering of  $U_C$  significantly increases the reward  $R$  and reduces the error of VQE energy (Figure 3(a) and (b)). Thus, the crucial aspect of our approach is the engineering of the Hamiltonian to maximize the initial energy gradients.

In Sec. 2.4, we have shown that naïve Clifford circuit optimization without proper engineering of  $U_C$  becomes inefficient as  $N$  increases. This trend is manifested by comparing Figure 3(c) and (d), in which extending from the active space treatment to full space treatment introduces significant challenges to maximizing  $R$ . Meanwhile, although in Figure 3(d) most of the cases have nearly zero  $R$  values, in Figure 3(b) most of the data points are close to the theoretical highest reward  $R_{\text{max}}$  and the energy errors are significantly lower than the ones in Figure 3(d). Such findings underscore the necessity of performing Hamiltonian engineering. Addi-

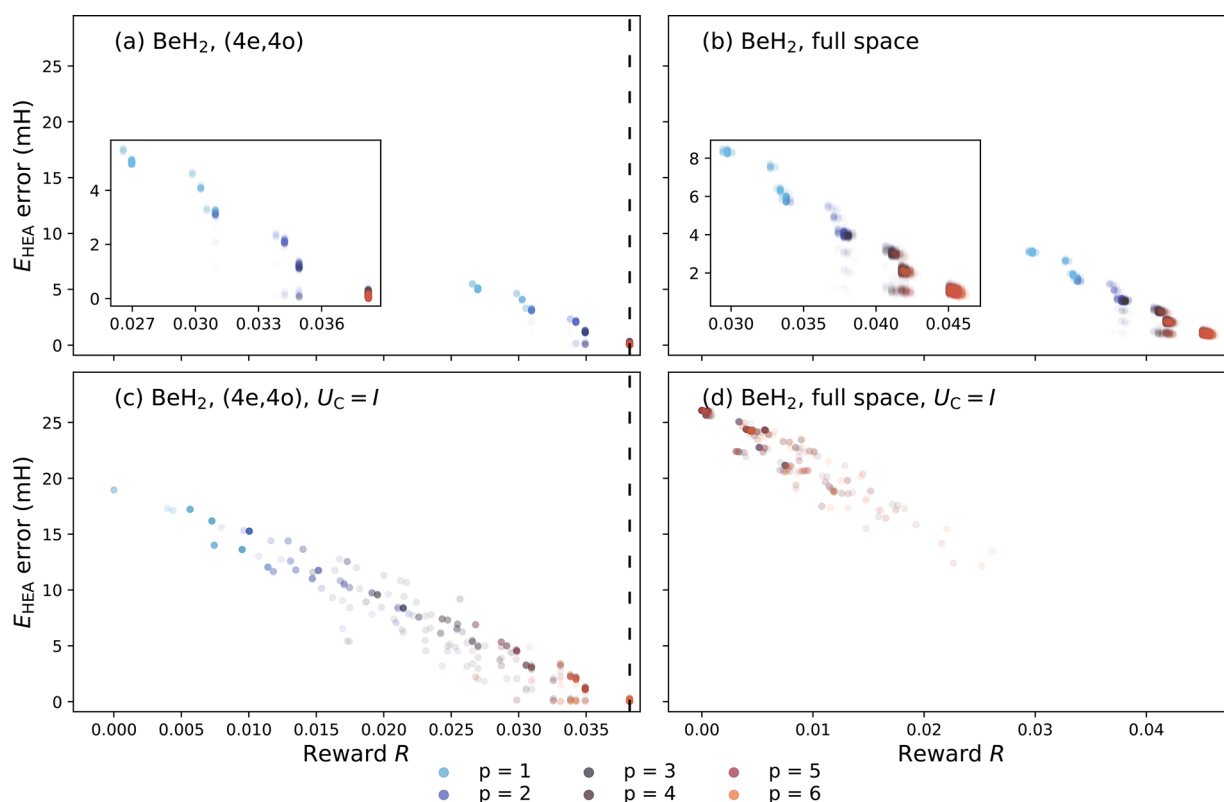


**Figure 3.** Errors of optimized HEA energies as a function of the reward  $R$  with and without Clifford-based Hamiltonian engineering using  $\text{BeH}_2$  systems as examples. In (a) and (c), the (4e, 4o) active space is employed, and in (b) and (d), the full space is employed. In top panels (a) and (b), the Hamiltonian engineering is performed, and in bottom panels (c) and (d), the Hamiltonian engineering is not performed. Optimized HEA energy errors are computed with the corresponding reference FCI energies. The dashed lines represent the theoretical highest reward  $R_{\text{max}}$  that the corresponding molecular system can reach. In each panel, for each circuit depth  $p$ , the results of 1000 trials with the corresponding labeled settings are plotted.

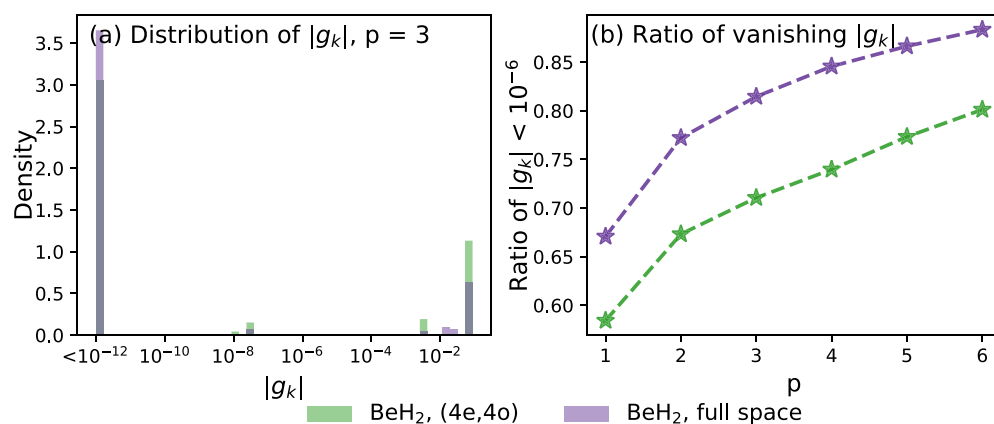


**Figure 4.** Distributions of gradients  $|g_k|$  obtained from CHEM for  $\text{BeH}_2$  systems calculated with (4e, 4o) and full space with different circuit depths. (a) The density histograms of the absolute values of the gradients with  $p = 3$  are shown in the plots ( $|g_k|$ ). To better display the small values, we plot the  $x$ -axes on logarithm scales. Additional histograms of  $|g_k|$  collected with different  $p$  values are shown in Supporting Information Figure S2. Panel (b) displays the ratio of  $|g_k|$  values smaller than  $10^{-6}$  versus the depth of the circuits  $p$  for two systems.

tionally, CHEM scales well with the number of layers  $p$  in the HEA circuit. In all the panels, the rewards tend to increase and lead to lower VQE energies with increasing  $p$  values.

**3.2. Potential Reduction of VQE Parameters.** Another advantage of the CHEM framework is that most of the  $g_k$  is zero as a result of eq 15, which implies their impacts on the energy minimization procedure may be neglected. The density histograms of  $g_k$  collected from 1000 CHEM trials with

different  $p$ 's are shown in Figure 4. The histograms show that a small fraction of the parameters contributes to most of the reward function  $R$ , and more than half of the parameters have nearly zero ( $|g_k| < 10^{-6}$ ) gradients. Figure 4(b) plots the ratios of parameters with vanishing gradients ( $|g_k| < 10^{-6}$ ) as a function of circuit depth  $p$ . This ratio increases when the number of qubits  $N$  or the circuit depth  $p$  increases by comparing the results of the simulations with (4e, 4o) and full

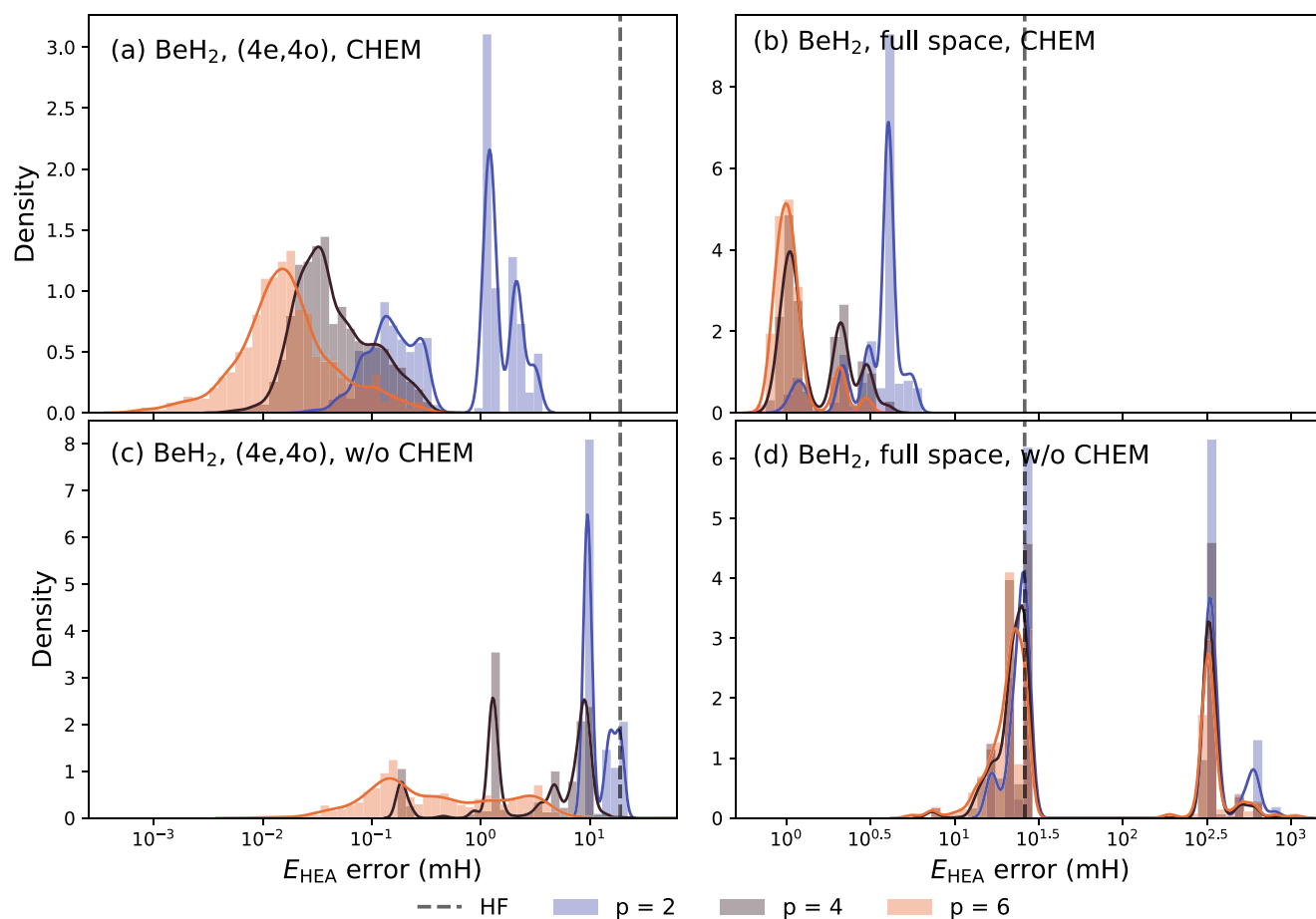


**Figure 5.** Optimized energy distributions using the **CHEM** protocol and  $R_y$  ansatz with random initializations for (a)  $\text{BeH}_2$  (4e,4o) and (b)  $\text{BeH}_2$  full space. In (c) and (d), the corresponding results for the  $R_y$  ansatz without **CHEM** are shown. The gray dashed vertical lines represent the corresponding errors for HF energy. The solid curves are from kernel density estimation (KDE).

**Table 2. Errors of Optimized HEA Energies with Respect to FCI for the  $\text{BeH}_2$  Molecule with Full Space<sup>b</sup>**

	w/o CHEM	CHEM	SA-free CHEM
MIN <sup>a</sup> (mH)	16.61	0.7954	0.914
MAE <sup>a</sup> (mH)	85.50	2.240	7.844
STD <sup>a</sup> (mH)	141.02	1.012	0.930

<sup>a</sup>†, MIN: minimum error. \*, MAE: mean absolute error. ‡, STD: standard deviation of the error. <sup>b</sup>The number of layers is set to 3. The three columns are for the  $R_y$  ansatz, **CHEM**, and **CHEM** without SA optimization from 1000 trials, respectively.

space and the results of the simulations with different  $p$  values, respectively. By fixing the parameters with zero gradients, a reduction of the dimensionality in the optimization problem can be achieved to significantly accelerate VQE optimizations. Incorporating this fact with more advanced optimization techniques, such as Bayesian optimizations,<sup>60</sup> could also enable efficient and noise-robust simulations on the near-term quantum devices, which is a future direction and is not taken into account in this work for simplicity.

**3.3. Comparison to HEA without CHEM.** Next, we compare the optimized energy from **CHEM** with traditional VQE based on the  $R_y$  ansatz. The  $R_y$  ansatz is a special form of HEA that allows only the  $R_y$  gates in the rotation layers  $L_{\text{rot}}$ .<sup>17,29,34,61</sup> The ansatz is popular for molecular electronic

structure simulations because it enforces real amplitude in the wave function. Due to optimization challenges associated with traditional HEA circuits, it is common to run VQE multiple times with different initial guesses in order to obtain meaningful results. In the following, the lowest energy obtained from 1000 independent trials is reported for the  $R_y$  ansatz. Since **CHEM** deterministically starts the optimization from  $\theta = 0$ , we also run **CHEM** 1000 times with random SA, corresponding to 1000 independent VQE optimizations, to ensure a fair comparison.

The distributions of the VQE optimized energies with  $p = 2, 4, 6$  are illustrated in **Figure 5**. The results with  $p = 1, 3, 5$  are included in **Supporting Information** Figure S5. In all cases considered, the results from **CHEM** outperform the results from the  $R_y$  ansatz by a considerable margin, as demonstrated in **Figure 5(b)** for the full space calculation of the  $\text{BeH}_2$  molecule. Since with **CHEM** the VQE optimization starts from the HF energy, the energy errors of **CHEM** are consistently lower than the ones of HF. The same is not true for traditional HEA, in which case the largest error is around 1 Hartree due to the poor initial guess. Additionally, the accuracy of **CHEM** monotonically increases as  $p$  increases from 2 to 6. In both panels of **Figure 5**, it is visible that **CHEM** can reach chemical accuracy (error < 1.6 mH) when  $p = 2$ . Intriguingly, we have observed unusual distributions of the optimized parameters for the  $R_y$  ansatz over the 1000 VQE runs, which is plotted in

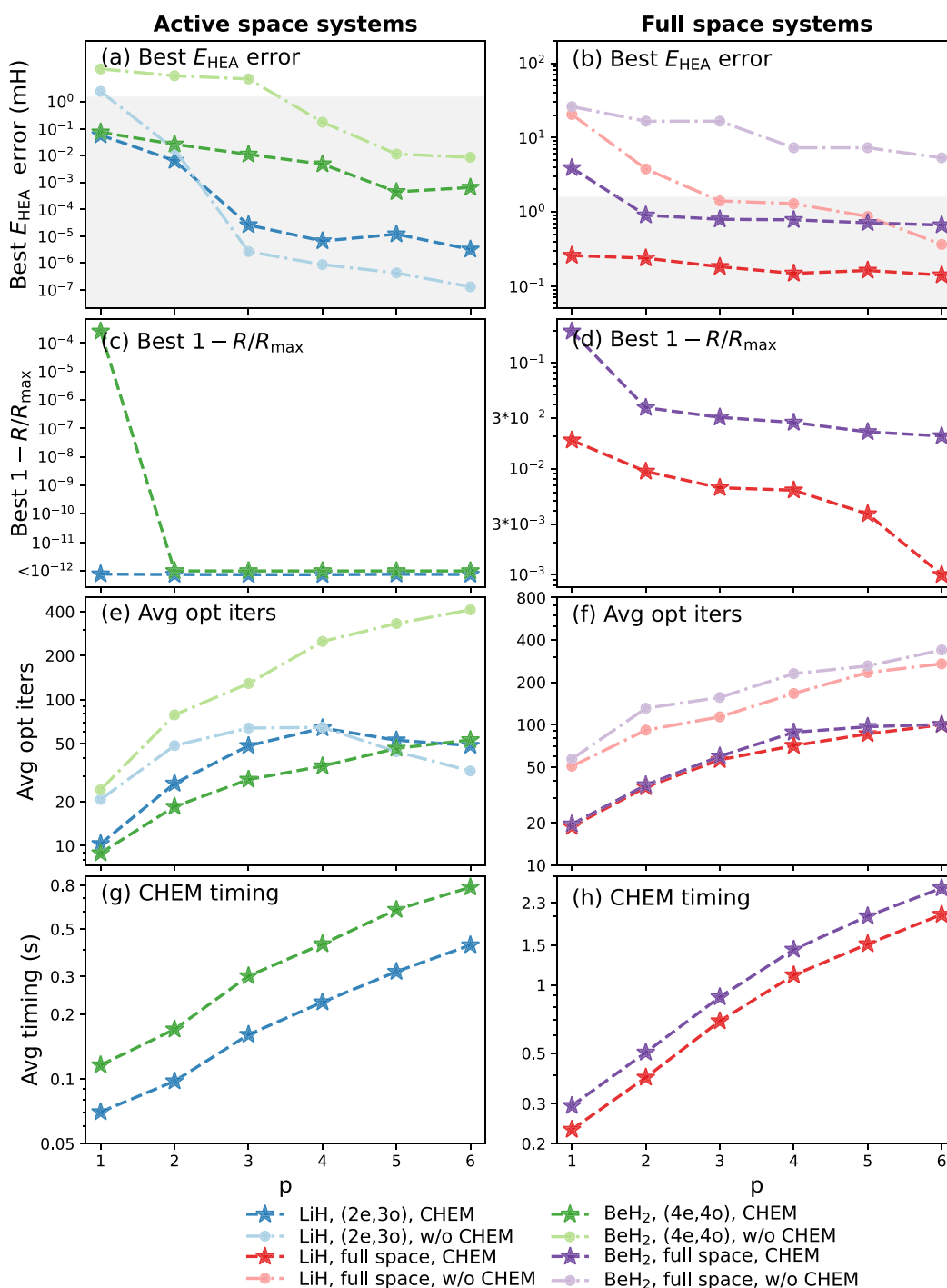


**Figure 6.** Optimized HEA energies (in (a) and (b)), reward function (in (c) and (d)), optimization costs (in (e) and (f)), and the wall time (in (g) and (h)) for CHEM with and without active space treatments of the three molecules. Lines with deep colors and star markers are for CHEM, and lines with light color and circle markers are for the VQE based on the Hamiltonian without Clifford transformation. All y axes are plotted on logarithm scales. The shaded areas in (a) and (b) correspond to the chemical accuracy of 1 kcal/mol (or 1.6 mH).

**Supporting Information** Figure S1. More specifically, most of the optimized parameters are close to integer or half-integer times of  $\pi$ , which turns the corresponding rotation gates  $R_y(\theta_j)$  into Clifford gates. In the **Supporting Information**, we discuss its potential connection to the remarkable efficiency of our method.

In **Table 2**, we present a comparison of error statistics between CHEM and the  $R_y$  ansatz. Consistent with the results

shown in **Figure 5**, CHEM significantly outperforms the  $R_y$  ansatz in terms of minimum error, absolute error, and standard deviation of error. Additionally, we include results from CHEM without SA optimization in **Table 2**. In this case, we employ the  $R_y$  ansatz and construct  $U_C$  from randomly chosen  $X_Q$  columns. While the accuracy of the SA-free method is expectedly lower than CHEM, the mean absolute error is only 10% of the  $R_y$  ansatz, and the minimum error is only 15%

**Table 3. Errors of Optimized HEA Energies and Required Average Numbers of Iterations Using Random Initialization and CHEM for Different Systems<sup>a,b</sup>**

System	No. of qubits	HF error (mH)	w/o CHEM $\times 1000$ ( $p=3$ )			CHEM $\times 1000$ ( $p=3$ )		
			MIN* (mH)	MAE <sup>†</sup> (mH)	ITER <sup>#</sup>	MIN (mH)	MAE (mH)	ITER
H <sub>4</sub> , (2e, 3o)	4	20.81	3.755e-06	4.763e-02	118.6	1.371e-07	2.412e-02	26.02
LiH, (2e, 3o)	4	19.21	2.656e-06	0.1514	63.89	2.608e-05	5.807e-02	48.31
BeH <sub>2</sub> , (4e, 4o)	6	18.97	7.242	10.57	128.8	1.115e-02	0.1445	28.39
H <sub>2</sub> O, (4e, 4o)	6	7.451	1.353	5.367	85.56	1.427e-05	2.824e-02	15.97
H <sub>4</sub> , full space	6	46.17	17.61	22.05	179.9	1.876e-02	0.8048	96.10
LiH, full space	10	20.46	1.405	36.83	113.6	0.1828	0.4897	56.20
BeH <sub>2</sub> , full space	12	26.07	16.61	85.50	156.1	0.7954	2.240	59.53

<sup>a</sup>\*, MIN: minimum error of the 1000 trials. <sup>†</sup>, MAE: mean absolute error of the 1000 trials. <sup>#</sup>, ITER: averaged number of iterations for VQE optimization. <sup>b</sup>The errors are computed using the FCI energies as references for the corresponding systems. Errors below chemical accuracy (about 1.6 mH) are marked in green.

higher than CHEM. Thus, the strength of CHEM lies in Hamiltonian engineering, and the SA optimization serves as an improvement component with very little additional cost (see Figure 6).

**3.4. Benchmark of Optimized VQE Energies.** We then examine the performance of CHEM by extensive benchmark over 7 different electronic structure problems, ranging from 4 qubits to 12 qubits. In Figure 6(a) and (b), we show the best error over 1000 different initializations based on both CHEM and the  $R_y$  ansatz. For simpler systems such as LiH with (2e, 3o) active space shown in Figure 6(a), both methods can achieve high accuracy. For larger systems such as BeH<sub>2</sub> without active space approximation, CHEM consistently outperforms the  $R_y$  ansatz. While the  $R_y$  ansatz without Hamiltonian engineering struggles to decrease the error below 10 mH, CHEM reaches chemical accuracy with  $p = 2$ . Since the number of CNOT gates in the circuit is  $(N - 1)p$  in our setting (Figure 1), CHEM drives the error below 1 mH with only 22 CNOT gates in the circuit. Note that the circuit used in Figure 1 has linear qubit connectivity which is the minimal requirement for the quantum hardware architecture. Upon increasing  $p$ , the best error from CHEM decreases at a slow pace. We conjecture that the origin of the slow pace is the saturation of the reward function  $R$  to  $R_{\max}$ . As shown in Figure 6(c) and (d), the optimized  $R$  is very close to the theoretical maximum value. For smaller systems employing active space approximation, the reward function  $R$  hardly changes with  $p$ , which is a possible reason for the fluctuation of best errors shown in Figure 6(a). Therefore, a possible direction to further improve CHEM when  $p$  becomes large is to design a more sophisticated  $R$  that acts as a more faithful proxy to the VQE-optimized energy. A straightforward approach without much additional complexity is to consider higher-order energy derivatives. One may notice that the circuit used for CHEM has more parameters than the  $R_y$  ansatz with a given number of layers  $p$  and expect the VQE optimization of CHEM to be more difficult than that of the  $R_y$  ansatz without CHEM. However, as shown in Figure 6(e) and (f), the optimization of CHEM takes fewer steps to converge due to the large initial gradients. For the LiH (2e, 3o) system, the benefits of our method, CHEM, are not as pronounced for larger  $p$  values due to the saturation of the reward function. However, it is important to note that this phenomenon is only observed in smaller systems where the optimization process does not present a significant challenge. Consequently, we believe that the impact of this occurrence on the practical application of VQE is minimal. Also, as shown in Figure 4, many parameters have zero gradients and can potentially be set as frozen during parameter optimization, which further reduces the optimization

difficulty. Lastly, we note that it is almost instant to perform CHEM in all cases reported (Figure 6(g) and (h)). Besides, the wall time scales linearly with  $p$ , in agreement with the formal scaling of  $O(N^2(N + p))$ .

In Table 3, we list the statistics of errors including the minimum error (MIN) and the mean absolute error (MAE) over the 7 different systems at  $p = 3$ . Due to the lack of a proper initial guess for traditional HEA, it is not trivial for the  $R_y$  ansatz to reach the HF energy. For example, the MAEs of full space LiH and BeH<sub>2</sub> are higher than the HF error when the  $R_y$  ansatz is employed, although their minimum errors are lower. On the other hand, CHEM starts the optimization from the HF energy with large energy gradients. As a result, the MAE of CHEM is much smaller than the HF error and reaches chemical accuracy except for the BeH<sub>2</sub> system. And if the minimum error is considered, chemical accuracy is reached for all systems studied in this work. The distributions of the optimized CHEM energies of the systems are included in the Supporting Information (Figures S3–S6).

#### 4. CONCLUSION AND OUTLOOK

In conclusion, we have developed a Clifford Hamiltonian Engineering for Molecules (CHEM) approach for highly accurate molecular energy estimation with shallow quantum circuits. By designing the Hamiltonian transformation  $U_{\text{CHEM}}$  that maximizes the energy gradient, CHEM remarkably alleviates the optimization difficulties associated with hardware-efficient ansatz without breaking the arbitrariness of the circuit topology. Based on the efficient algorithmic implementation, CHEM bears minimal classical computing overhead, with a computational complexity of  $O(N^2(N + p))$ , and no additional quantum resources are needed. The numerical experimental results for a variety of molecular systems show that our approach scales well with both  $N$  and  $p$ . In particular, we find CHEM reaches chemical accuracy for these molecules using quantum circuits with fewer than 30 two-qubit gates and linear qubit connectivity. This level of performance is unprecedented in the literature and highlights the potential of our method for practical applications in quantum computational chemistry.

Looking forward, there are several avenues for further research and development. First, by designing a more sophisticated reward function  $R$  and a better algorithm to match  $x_h$  and  $x_Q$ , it is possible to further improve the performance of CHEM. Second, integrating CHEM with other optimization techniques and ansatzes could lead to even more efficient and accurate quantum algorithms. Finally, the implementation of our Clifford Hamiltonian engineering

approach on real quantum hardware would provide valuable insights into its performance and robustness in the presence of hardware noise.

It is intriguing to contemplate the potential application of CHEM to long-term quantum algorithms, such as quantum phase estimation (QPE) and adiabatic state preparation (ASP). In the context of QPE, increasing the overlap between the trial wave function and the ground state presents a significant challenge. In this scenario, both VQE and CHEM could provide good input for QPE by generating accurate trial wave functions. On the other hand, the success of ASP is dependent on maintaining a large energy gap along the evolution path. Since CHEM preserves the eigenspectrum, an effective strategy to utilize CHEM for ASP deserves further investigation.

Overall, our work contributes to the ongoing efforts to develop efficient and accurate quantum algorithms for chemistry applications and brings us one step closer to unleashing the full potential of quantum computational chemistry on near-term quantum devices.

## ■ ASSOCIATED CONTENT

### Data Availability Statement

All graphs and results presented in this study are shared on a GitHub repository (<https://github.com/sherrylixuecheng/CHEM>). The additional figures for test results are shown in the Supporting Information, and full accuracy statistics are included in a separate excel (Supplementary Data). Code availability: The entire CHEM framework is available on GitHub (<https://github.com/sherrylixuecheng/CHEM>) with example jupyter notebooks and all the testing results. The example codes to perform HEA simulations are available on TENCIRCHEM (<https://github.com/tencent-quantum-lab/tencirchem>).<sup>54</sup>

### SI Supporting Information

The Supporting Information is available free of charge at <https://pubs.acs.org/doi/10.1021/acs.jctc.3c00886>.

Distributions of the optimized parameters of the  $R_y$  ansatz and distributions of the energy gradients and optimized energies of the CHEM method (PDF)

## ■ AUTHOR INFORMATION

### Corresponding Author

Weitang Li – Tencent Quantum Lab, Shenzhen 518057, China; [orcid.org/0000-0002-8739-641X](https://orcid.org/0000-0002-8739-641X);  
Email: [liw31@gmail.com](mailto:liw31@gmail.com)

### Authors

Jiace Sun – Division of Chemistry and Chemical Engineering, California Institute of Technology, Pasadena, California 91125, United States

Lixue Cheng – Division of Chemistry and Chemical Engineering, California Institute of Technology, Pasadena, California 91125, United States; [orcid.org/0000-0002-7329-0585](https://orcid.org/0000-0002-7329-0585)

Complete contact information is available at: <https://pubs.acs.org/doi/10.1021/acs.jctc.3c00886>

### Author Contributions

J.S. and L.W. developed the idea and implemented the codes. L.C. performed the numerical experiments. J.S., L.C., and L.W. analyzed the results and wrote the manuscript.

## Notes

The authors declare no competing financial interest.

## ■ ACKNOWLEDGMENTS

Jiace Sun is thankful for the support from the Hongyan Scholarship.

## ■ REFERENCES

- (1) Cao, Y.; Romero, J.; Olson, J. P.; Degroote, M.; Johnson, P. D.; Kieferová, M.; Kivlichan, I. D.; Menke, T.; Peropadre, B.; Sawaya, N. P.; Sim, S.; Veis, L.; Aspuru-Guzik, A. Quantum chemistry in the age of quantum computing. *Chem. Rev.* **2019**, *119*, 10856–10915.
- (2) Bauer, B.; Bravyi, S.; Motta, M.; Chan, G. K.-L. Quantum algorithms for quantum chemistry and quantum materials science. *Chem. Rev.* **2020**, *120*, 12685–12717.
- (3) McArdle, S.; Endo, S.; Aspuru-Guzik, A.; Benjamin, S. C.; Yuan, X. Quantum computational chemistry. *Rev. Mod. Phys.* **2020**, *92*, 015003.
- (4) Motta, M.; Rice, J. E. Emerging quantum computing algorithms for quantum chemistry. *Wiley Interdiscip. Rev. Comput. Mol. Sci.* **2022**, *12*, e1580.
- (5) Liu, J.; Fan, Y.; Li, Z.; Yang, J. Quantum algorithms for electronic structures: basis sets and boundary conditions. *Chem. Soc. Rev.* **2022**, *51*, 3263–3279.
- (6) Ma, H.; Liu, J.; Shang, H.; Fan, Y.; Li, Z.; Yang, J. Multiscale quantum algorithm for quantum chemistry. *Chem. Sci.* **2023**, *14*, 3190–3205.
- (7) Peruzzo, A.; McClean, J.; Shadbolt, P.; Yung, M.-H.; Zhou, X.-Q.; Love, P. J.; Aspuru-Guzik, A.; O'Brien, J. L. A variational eigenvalue solver on a photonic quantum processor. *Nat. Commun.* **2014**, *5*, 4213.
- (8) Cerezo, M.; Arrasmith, A.; Babbush, R.; Benjamin, S. C.; Endo, S.; Fujii, K.; McClean, J. R.; Mitarai, K.; Yuan, X.; Cincio, L.; Coles, P. J. Variational quantum algorithms. *Nat. Rev. Phys.* **2021**, *3*, 625–644.
- (9) Tilly, J.; Chen, H.; Cao, S.; Picozzi, D.; Setia, K.; Li, Y.; Grant, E.; Wossnig, L.; Rungger, I.; Booth, G. H.; Tennyson, J. The variational quantum eigensolver: a review of methods and best practices. *Phys. Rep.* **2022**, *986*, 1–128.
- (10) Preskill, J. Quantum Computing in the NISQ era and beyond. *Quantum* **2018**, *2*, 79.
- (11) Bharti, K.; Cervera-Lierta, A.; Kyaw, T. H.; Haug, T.; Alperin-Lea, S.; Anand, A.; Degroote, M.; Heimonen, H.; Kottmann, J. S.; Menke, T.; Mok, W.-K.; Sim, S.; Kwok, L.-C.; Aspuru-Guzik, A. Noisy intermediate-scale quantum algorithms. *Rev. Mod. Phys.* **2022**, *94*, 015004.
- (12) Kandala, A.; Mezzacapo, A.; Temme, K.; Takita, M.; Brink, M.; Chow, J. M.; Gambetta, J. M. Hardware-efficient variational quantum eigensolver for small molecules and quantum magnets. *Nature* **2017**, *549*, 242–246.
- (13) Google AI Quantum and Collaborators; Arute, F.; Arya, K.; Babbush, R.; Bacon, D.; Bardin, J. C.; Barends, R.; Boixo, S.; Broughton, M.; Buckley, B. B.; Buell, D. A.; Burkett, B.; Bushnell, N.; Chen, Y.; Chen, Z.; Chiaro, B.; Collins, R.; Courtney, W.; Demura, S.; Dunsworth, A.; Farhi, E.; Fowler, A.; Foxen, B.; Gidney, C.; Giustina, M.; Graff, R.; Habegger, S.; Harrigan, M. P.; Ho, A.; Hong, S.; Huang, T.; Huggins, W. J.; Ioffe, L.; Isakov, S. V.; Jeffrey, E.; Jiang, Z.; Jones, C.; Kafri, D.; Kechedzhi, K.; Kelly, J.; Kim, S.; Klimov, P. V.; Korotkov, A.; Kostrietsa, F.; Landhuis, D.; Laptev, P.; Lindmark, M.; Lucero, E.; Martin, O.; Martinis, J. M.; McClean, J. R.; McEwen, M.; Megrant, A.; Mi, X.; Mohseni, M.; Mruczkiewicz, W.; Mutus, J.; Naaman, O.; Neeley, M.; Neill, C.; Neven, H.; Niu, M. Y.; O'Brien, T. E.; Ostby, E.; Petukhov, A.; Putterman, H.; Quintana, C.; Roushan, P.; Rubin, N. C.; Sank, D.; Satzinger, K. J.; Smelyanskiy, V.; Strain, D.; Sung, K. J.; Szalay, M.; Takeshita, T. Y.; Vainsencher, A.; White, T.; Wiebe, N.; Yao, Z. J.; Yeh, P.; Zalcman, A.; et al. Hartree-Fock on a superconducting qubit quantum computer. *Science* **2020**, *369*, 1084–1089.

- (14) O'Brien, T. E.; Anselmetti, G.; Gkritsis, F.; Elfving, V. E.; Polla, S.; Huggins, W. J.; Oumarou, O.; Kechedzhi, K.; Abanin, D.; Acharya, R.; Aleiner, I.; Allen, R.; Andersen, T. I.; Anderson, K.; Ansmann, M.; Arute, F.; Arya, K.; Asfaw, A.; Atalaya, J.; Bardin, J. C.; Bengtsson, A.; Bortoli, G.; Bourassa, A.; Bovaird, J.; Brill, L.; Broughton, M.; Buckley, B.; Buell, D. A.; Burger, T.; Burkett, B.; Bushnell, N.; Campero, J.; Chen, Z.; Chiaro, B.; Chik, D.; Cogan, J.; Collins, R.; Conner, P.; Courtney, W.; Crook, A. L.; Curtin, B.; Debroy, D. M.; Demura, S.; Drozdov, I.; Dunsworth, A.; Erickson, C.; Faoro, L.; Farhi, E.; Fatemi, R.; Ferreira, V. S.; Flores Burgos, L.; Forati, E.; Fowler, A. G.; Foxen, B.; Giang, W.; Gidney, C.; Gilboa, D.; Giustina, M.; Gosula, R.; Grajales Dau, A.; Gross, J. A.; Habegger, S.; Hamilton, M. C.; Hansen, M.; Harrigan, M. P.; Harrington, S. D.; Heu, P.; Hoffmann, M. R.; Hong, S.; Huang, T.; Huff, A.; Ioffe, L. B.; Isakov, S. V.; Iveland, J.; Jeffrey, E.; Jiang, Z.; Jones, C.; Juhas, P.; Kafri, D.; Khattar, T.; Khezri, M.; Kieferová, M.; Kim, S.; Klimov, P. V.; Klots, A. R.; Korotkov, A. N.; Kostritsa, F.; Kreikebaum, J. M.; Landhuis, D.; Laptev, P.; Lau, K.-M.; Laws, L.; Lee, J.; Lee, K.; Lester, B. J.; Lill, A. T.; Liu, W.; Livingston, W. P.; Locharla, A.; Malone, F. D.; Mandrà, S.; Martin, O.; Martin, S.; McClean, J. R.; McCourt, T.; McEwen, M.; Mi, X.; Mieszala, A.; Miao, K. C.; Mohseni, M.; Montazeri, S.; Morvan, A.; Movassagh, R.; Mruzckiewicz, W.; Naaman, O.; Neeley, M.; Neill, C.; Nersisyan, A.; Newman, M.; Ng, J. H.; Nguyen, A.; Nguyen, M.; Niu, M. Y.; Omonije, S.; Opremcak, A.; Petukhov, A.; Potter, R.; Pryadko, L. P.; Quintana, C.; Rocque, C.; Roushan, P.; Saei, N.; Sank, D.; Sankaragomathi, K.; Satzinger, K. J.; Schurkus, H. F.; Schuster, C.; Shearn, M. J.; Shorter, A.; Shutt, N.; Shvarts, V.; Skrzuzny, J.; Smith, W. C.; Somma, R. D.; Sterling, G.; Strain, D.; Szalay, M.; Thor, D.; Torres, A.; Vidal, G.; Villalonga, B.; Vollgraff Heidweiller, C.; White, T.; Woo, B. W. K.; Xing, C.; Yao, Z. J.; Yeh, P.; Yoo, J.; Young, G.; Zalcman, A.; Zhang, Y.; Zhu, N.; Zobrist, N.; Bacon, D.; Boixo, S.; Chen, Y.; Hilton, J.; Kelly, J.; Lucero, E.; Megrant, A.; Neven, H.; Smelyanskiy, V.; Gogolin, C.; Babbush, R.; Rubin, N. C. Purification-based quantum error mitigation of pair-correlated electron simulations. *arXiv:2210.10799 arXiv preprint* 2022. <https://arxiv.org/abs/2210.10799> (accessed 2023-12-29).
- (15) Guo, S.; Sun, J.; Qian, H.; Gong, M.; Zhang, Y.; Chen, F.; Ye, Y.; Wu, Y.; Cao, S.; Liu, K.; Zha, C.; Ying, C.; Zhu, Q.; Huang, H.-L.; Zhao, Y.; Li, S.; Wang, S.; Yu, J.; Fan, D.; Wu, D.; Su, H.; Deng, H.; Rong, H.; Li, Y.; Zhang, K.; Chung, T.-H.; Liang, F.; Lin, J.; Xu, Y.; Sun, L.; Guo, C.; Li, N.; Huo, Y.-H.; Peng, C.-Z.; Lu, C.-Y.; Yuan, X.; Zhu, X.; Pan, J.-W. Experimental quantum computational chemistry with optimized unitary coupled cluster ansatz. *arXiv:2212.08006 arXiv preprint* 2022. <https://arxiv.org/abs/2212.08006> (accessed 2023-12-29).
- (16) Barkoutsos, P. K.; Gkritsis, F.; Ollitrault, P. J.; Sokolov, I. O.; Woerner, S.; Tavernelli, I. Quantum algorithm for alchemical optimization in material design. *Chem. Sci.* **2021**, *12*, 4345–4352.
- (17) Gao, Q.; Jones, G. O.; Motta, M.; Sugawara, M.; Watanabe, H. C.; Kobayashi, T.; Watanabe, E.; Ohnishi, Y.-y.; Nakamura, H.; Yamamoto, N. Applications of quantum computing for investigations of electronic transitions in phenylsulfonfyl-carbazole TADF emitters. *npj Comput. Mater.* **2021**, *7*, 70.
- (18) Li, W.; Huang, Z.; Cao, C.; Huang, Y.; Shuai, Z.; Sun, X.; Sun, J.; Yuan, X.; Lv, D. Toward practical quantum embedding simulation of realistic chemical systems on near-term quantum computers. *Chem. Sci.* **2022**, *13*, 8953–8962.
- (19) Malone, F. D.; Parrish, R. M.; Welden, A. R.; Fox, T.; Degroote, M.; Kyoseva, E.; Moll, N.; Santagati, R.; Streif, M. Towards the simulation of large scale protein-ligand interactions on NISQ-era quantum computers. *Chem. Sci.* **2022**, *13*, 3094–3108.
- (20) Motta, M.; Jones, G. O.; Rice, J. E.; Gujarati, T. P.; Sakuma, R.; Liepuoniute, I.; Garcia, J. M.; Ohnishi, Y.-y. Quantum chemistry simulation of ground-and excited-state properties of the sulfonium cation on a superconducting quantum processor. *Chem. Sci.* **2023**, *14*, 2915–2927.
- (21) McClean, J. R.; Romero, J.; Babbush, R.; Aspuru-Guzik, A. The theory of variational hybrid quantum-classical algorithms. *New J. Phys.* **2016**, *18*, 023023.
- (22) Fedorov, D. A.; Peng, B.; Govind, N.; Alexeev, Y. VQE method: a short survey and recent developments. *Mater. Theory* **2022**, *6*, 2.
- (23) Lee, J.; Huggins, W. J.; Head-Gordon, M.; Whaley, K. B. Generalized unitary coupled cluster wave functions for quantum computation. *J. Chem. Theory and Comput.* **2019**, *15*, 311–324.
- (24) Gard, B. T.; Zhu, L.; Barron, G. S.; Mayhall, N. J.; Economou, S. E.; Barnes, E. Efficient symmetry-preserving state preparation circuits for the variational quantum eigensolver algorithm. *npj Quantum Inf.* **2020**, *6*, 10.
- (25) Anselmetti, G.-L. R.; Wierichs, D.; Gogolin, C.; Parrish, R. M. Local, expressive, quantum-number-preserving VQE ansätze for fermionic systems. *New J. Phys.* **2021**, *23*, 113010.
- (26) Xiao, X.; Zhao, H.; Ren, J.; Fang, W.-h.; Li, Z. Physics-constrained hardware-efficient ansatz on quantum computers that is universal, systematically improvable, and size-consistent. *arXiv:2307.03563 arXiv preprint* 2023. <https://arxiv.org/abs/2307.03563> (accessed 2023-12-29).
- (27) Anand, A.; Schleich, P.; Alperin-Lea, S.; Jensen, P. W.; Sim, S.; Díaz-Tinoco, M.; Kottmann, J. S.; Degroote, M.; Izmaylov, A. F.; Aspuru-Guzik, A. A quantum computing view on unitary coupled cluster theory. *Chem. Soc. Rev.* **2022**, *51*, 1659–1684.
- (28) Kandala, A.; Temme, K.; Córcoles, A. D.; Mezzacapo, A.; Chow, J. M.; Gambetta, J. M. Error mitigation extends the computational reach of a noisy quantum processor. *Nature* **2019**, *567*, 491–495.
- (29) Gao, Q.; Nakamura, H.; Gujarati, T. P.; Jones, G. O.; Rice, J. E.; Wood, S. P.; Pistoia, M.; Garcia, J. M.; Yamamoto, N. Computational investigations of the lithium superoxide dimer rearrangement on noisy quantum devices. *J. Phys. Chem. A* **2021**, *125*, 1827–1836.
- (30) Kirsopp, J. J.; Di Paola, C.; Manrique, D. Z.; Krompiec, M.; Greene-Diniz, G.; Guba, W.; Meyder, A.; Wolf, D.; Strahm, M.; Muñoz Ramo, D. Quantum computational quantification of protein-ligand interactions. *Int. J. Quantum Chem.* **2022**, *122*, e26975.
- (31) O'Malley, P. J. J.; Babbush, R.; Kivlichan, I. D.; Romero, J.; McClean, J. R.; Barends, R.; Kelly, J.; Roushan, P.; Tranter, A.; Ding, N.; Campbell, B.; Chen, Y.; Chen, Z.; Chiaro, B.; Dunsworth, A.; Fowler, A. G.; Jeffrey, E.; Lucero, E.; Megrant, A.; Mutus, J. Y.; Neeley, M.; Neill, C.; Quintana, C.; Sank, D.; Vainsencher, A.; Wenner, J.; White, T. C.; Coveney, P. V.; Love, P. J.; Neven, H.; Aspuru-Guzik, A.; Martinis, J. M. Scalable quantum simulation of molecular energies. *Phys. Rev. X* **2016**, *6*, 031007.
- (32) Nam, Y.; Chen, J.-S.; Pisenti, N. C.; Wright, K.; Delaney, C.; Maslov, D.; Brown, K. R.; Allen, S.; Amini, J. M.; Apisdorf, J.; Beck, K. M.; Blinov, A.; Chaplin, V.; Chmielewski, M.; Collins, C.; Debnath, S.; Hudek, K. M.; Ducore, A. M.; Keesan, M.; Kreikemeier, S. M.; Mizrahi, J.; Solomon, P.; Williams, M.; Wong-Campos, J. D.; Moehring, D.; Monroe, C.; Kim, J. Ground-state energy estimation of the water molecule on a trapped-ion quantum computer. *npj Quantum Inf.* **2020**, *6*, 33.
- (33) McClean, J. R.; Boixo, S.; Smelyanskiy, V. N.; Babbush, R.; Neven, H. Barren plateaus in quantum neural network training landscapes. *Nat. Commun.* **2018**, *9*, 4812.
- (34) Choy, B.; Wales, D. J. Molecular energy landscapes of hardware-efficient ansatz in quantum computing. *J. Chem. Theory and Comput.* **2023**, *19*, 1197–1206.
- (35) Grimsley, H. R.; Economou, S. E.; Barnes, E.; Mayhall, N. J. An adaptive variational algorithm for exact molecular simulations on a quantum computer. *Nat. Commun.* **2019**, *10*, 3007.
- (36) Yordanov, Y. S.; Armaos, V.; Barnes, C. H.; Arvidsson-Shukur, D. R. Qubit-excitation-based adaptive variational quantum eigensolver. *Commun. Phys.* **2021**, *4*, 228.
- (37) Tang, H. L.; Shkolnikov, V.; Barron, G. S.; Grimsley, H. R.; Mayhall, N. J.; Barnes, E.; Economou, S. E. qubit-ADAPT-VQE: An adaptive algorithm for constructing hardware-efficient ansätze on a quantum processor. *PRX Quantum* **2021**, *2*, 020310.
- (38) Mizukami, W.; Mitarai, K.; Nakagawa, Y. O.; Yamamoto, T.; Yan, T.; Ohnishi, Y.-y. Orbital optimized unitary coupled cluster theory for quantum computer. *Phys. Rev. Res.* **2020**, *2*, 033421.

- (39) Sokolov, I. O.; Barkoutsos, P. K.; Ollitrault, P. J.; Greenberg, D.; Rice, J.; Pistoia, M.; Tavernelli, I. Quantum orbital-optimized unitary coupled cluster methods in the strongly correlated regime: Can quantum algorithms outperform their classical equivalents? *J. Chem. Phys.* **2020**, *152*, 124107.
- (40) Bierman, J.; Li, Y.; Lu, J. Improving the accuracy of variational quantum eigensolvers with fewer qubits using orbital optimization. *J. Chem. Theory Comput.* **2023**, *19*, 790–798.
- (41) Gottesman, D. The Heisenberg representation of quantum computers. quant-ph/9807006 *arXiv preprint* 1998. <https://arxiv.org/abs/quant-ph/9807006> (accessed 2023-12-29).
- (42) Aaronson, S.; Gottesman, D. Improved simulation of stabilizer circuits. *Phys. Rev. A* **2004**, *70*, 052328.
- (43) Leone, L.; Oliviero, S. F.; Cincio, L.; Cerezo, M. On the practical usefulness of the hardware efficient ansatz. *arXiv:2211.01477 arXiv preprint* 2022. <https://arxiv.org/abs/2211.01477> (accessed 2023-12-29).
- (44) Ryabinkin, I. G.; Yen, T.-C.; Genin, S. N.; Izmaylov, A. F. Qubit coupled cluster method: a systematic approach to quantum chemistry on a quantum computer. *J. Chem. Theory and Comput.* **2018**, *14*, 6317–6326.
- (45) Ryabinkin, I. G.; Lang, R. A.; Genin, S. N.; Izmaylov, A. F. Iterative qubit coupled cluster approach with efficient screening of generators. *J. Chem. Theory Comput.* **2020**, *16*, 1055–1063.
- (46) Ryabinkin, I. G.; Izmaylov, A. F.; Genin, S. N. A posteriori corrections to the iterative qubit coupled cluster method to minimize the use of quantum resources in large-scale calculations. *Quantum Sci. Technol.* **2021**, *6*, 024012.
- (47) Lang, R. A.; Ryabinkin, I. G.; Izmaylov, A. F. Unitary transformation of the electronic Hamiltonian with an exact quadratic truncation of the Baker-Campbell-Hausdorff expansion. *J. Chem. Theory and Comput.* **2021**, *17*, 66–78.
- (48) Genin, S. N.; Ryabinkin, I. G.; Paisley, N. R.; Whelan, S. O.; Helander, M. G.; Hudson, Z. M. Estimating phosphorescent emission energies in Ir<sup>III</sup> complexes using large-scale quantum computing simulations. *Angew. Chem., Int. Ed.* **2022**, *61*, e202116175.
- (49) Ryabinkin, I. G.; Jena, A. J.; Genin, S. N. Efficient construction of involutory linear combinations of anticommuting pauli generators for large-scale iterative qubit coupled cluster calculations. *J. Chem. Theory and Comput.* **2023**, *19*, 1722–1733.
- (50) Mishmash, R. V.; Gujarati, T. P.; Motta, M.; Zhai, H.; Chan, G. K.; Mezzacapo, A. Hierarchical Clifford transformations to reduce entanglement in quantum chemistry wavefunctions. *arXiv:2301.07726 arXiv preprint* 2023. <https://arxiv.org/abs/2301.07726> (accessed 2023-12-29).
- (51) Schleich, P.; Boen, J.; Cincio, L.; Anand, A.; Kottmann, J. S.; Tretiak, S.; Dub, P. A.; Aspuru-Guzik, A. Partitioning Quantum Chemistry Simulations with Clifford Circuits. *arXiv:2303.01221 arXiv preprint* 2023. <https://arxiv.org/abs/2303.01221> (accessed 2023-12-29).
- (52) Cheng, M.; Khosla, K.; Self, C.; Lin, M.; Li, B.; Medina, A.; Kim, M. Clifford circuit initialisation for variational quantum algorithms. *arXiv:2207.01539 arXiv preprint* 2022. <https://arxiv.org/abs/2207.01539> (accessed 2023-12-29).
- (53) Mitarai, K.; Suzuki, Y.; Mizukami, W.; Nakagawa, Y. O.; Fujii, K. Quadratic Clifford expansion for efficient benchmarking and initialization of variational quantum algorithms. *Phys. Rev. Res.* **2022**, *4*, 033012.
- (54) Li, W.; Allcock, J.; Cheng, L.; Zhang, S.-X.; Chen, Y.-Q.; Mailoa, J. P.; Shuai, Z.; Zhang, S. TenCirChem: An Efficient quantum computational chemistry package for the NISQ era. *J. Chem. Theory Comput.* **2023**, *19*, 3966.
- (55) Sun, Q.; Berkelbach, T. C.; Blunt, N. S.; Booth, G. H.; Guo, S.; Li, Z.; Liu, J.; McClain, J.; Sayfutyarova, E. R.; Sharma, S.; Wouters, S.; Chan, G. K.-L. PySCF: the Python-based simulations of chemistry framework. *Wiley Interdiscip. Rev. Comput. Mol. Sci.* **2018**, *8*, e1340.
- (56) Bravyi, S. B.; Kitaev, A. Y. Fermionic quantum computation. *Ann. Phys.* **2002**, *298*, 210–226.
- (57) Seeley, J. T.; Richard, M. J.; Love, P. J. The Bravyi-Kitaev transformation for quantum computation of electronic structure. *J. Chem. Phys.* **2012**, *137*, 224109.
- (58) Bradbury, J.; Frostig, R.; Hawkins, P.; Johnson, M. J.; Leary, C.; Maclaurin, D.; Necula, G.; Paszke, A.; VanderPlas, J.; Wanderman-Milne, S.; Zhang, Q. JAX: composable transformations of Python +NumPy programs. 2018. <http://github.com/google/jax> (accessed 2023-12-02).
- (59) Virtanen, P.; Gommers, R.; Oliphant, T. E.; Haberland, M.; Reddy, T.; Cournapeau, D.; Burovski, E.; Peterson, P.; Weckesser, W.; Bright, J.; van der Walt, S. J.; Brett, M.; Wilson, J.; Millman, K. J.; Mayorov, N.; Nelson, A. R. J.; Jones, E.; Kern, R.; Larson, E.; Carey, C. J.; Polat, I.; Feng, Y.; Moore, E. W.; VanderPlas, J.; Laxalde, D.; Perktold, J.; Cimrman, R.; Henriksen, I.; Quintero, E. A.; Harris, C. R.; Archibald, A. M.; Ribeiro, A. H.; Pedregosa, F.; van Mulbregt, P.; et al. SciPy 1.0 Contributors SciPy 1.0: Fundamental algorithms for scientific computing in python. *Nat. Methods* **2020**, *17*, 261–272.
- (60) Cheng, L.; Chen, Y.-Q.; Zhang, S.-X.; Zhang, S. Error-mitigated quantum approximate optimization via learning-based adaptive optimization. *arXiv:2303.14877 arXiv preprint* 2023. <https://arxiv.org/abs/2303.14877> (accessed 2023-12-29).
- (61) Miháliková, I.; Pivoluska, M.; Plesch, M.; Friák, M.; Nagaj, D.; Šob, M. The cost of improving the precision of the variational quantum eigensolver for quantum chemistry. *Nanomater* **2022**, *12*, 243.

## Recommended by ACS

### Quantum Neural Network Inspired Hardware Adaptable Ansatz for Efficient Quantum Simulation of Chemical Systems

Xiongzi Zeng, Jinlong Yang, *et al.*

DECEMBER 04, 2023

JOURNAL OF CHEMICAL THEORY AND COMPUTATION

READ 

### Growth Reduction of Similarity-Transformed Electronic Hamiltonians in Qubit Space

Robert A. Lang, Artur F. Izmaylov, *et al.*

SEPTEMBER 16, 2023

JOURNAL OF CHEMICAL THEORY AND COMPUTATION

READ 

### Efficient Mean-Field Simulation of Quantum Circuits Inspired by Density Functional Theory

Marco Bernardi.

NOVEMBER 10, 2023

JOURNAL OF CHEMICAL THEORY AND COMPUTATION

READ 

### Deep Neural Network Assisted Quantum Chemistry Calculations on Quantum Computers

Kalpaka Ghosh, Sharma S. R. K. C. Yamijjala, *et al.*

DECEMBER 04, 2023

ACS OMEGA

READ 

Get More Suggestions >